Microwave Engineering
Ulm University

universität ulm

Coded OFDM Waveforms for MIMO Radars

Christina Knill, Felix Embacher, Benedikt Schweizer, Simon Stephany, and Christian Waldschmidt

DOI: 10.1109/TVT.2021.3073268

Coded OFDM Waveforms for MIMO Radars

Christina Knill, *Graduate Student Member, IEEE,* Felix Embacher, Benedikt Schweizer, *Graduate Student Member, IEEE,* Simon Stephany, and Christian Waldschmidt, *Member, IEEE*

***Abstract*—Emerging digital radar concepts such as orthogonal frequency-division multiplexing (OFDM) allow flexible signal generation. This opens up new opportunities in waveform design in a multiple-input multiple-output (MIMO) system such as introducing coding for signal multiplexing. In this article, coded MIMO OFDM waveforms are proposed and investigated that allow continuous and simultaneous wideband transmission for all transmitters of a multiple transmit and receive antenna array for spatial radar environment perception. Challenges for coded MIMO OFDM radar operation are derived, and three coded MIMO strategies are introduced and analyzed. Their potential is validated and compared to the standard subcarrier interleaving OFDM approach using simulations and measurements of an experimental 4×4 MIMO OFDM radar at 77 GHz.**

***Index Terms*—OFDM, MIMO, radar, coding, CDM, FDM, TDM, STC, interleaving, auto-correlation, cross-correlation**

I. Introduction

FUTURE generation radar sensors should not only be able to accurately and robustly measure range and velocity of objects but also provide detailed angular information to allow a more pictorial spatial image of their environment [1]. For spatial imaging, multi-channel systems are required using multiple antennas at both transmitter and receiver. Multiple-input multiple-output (MIMO) systems achieve increased angular resolution through a large virtual aperture [2]. However, the use of several transmitters places new demands on the transmitted signals, as each transmitter should be clearly identifiable at the receiver, and self-interference due to channel cross-talk should be as low as possible or avoided completely. Typically, this is achieved by employing orthogonal transmission schemes such as time-division multiplexing (TDM), frequency-division multiplexing (FDM), or code-division multiplexing (CDM) [3].

In the last years, pushed by developments in CMOS technologies, novel digitally modulated radar concepts such as orthogonal frequency-division multiplexing (OFDM) [4]–[6] and phase-modulated continuous wave (PMCW) [7] have matured. Digital wideband OFDM modulation allows flexible signal generation and straightforward signal processing based on the Fourier transform. MIMO OFDM concepts commonly utilize an interleaved FDM scheme [8]–[10]. The standard approach uses linear interleaving [8], where the orthogonal subcarriers are periodically assigned to the transmit antennas that then can operate simultaneously and continuously. Yet, the periodical assignment of subcarriers to the transmit antennas results in ambiguities in range dimension and thereby in a reduced maximum unambiguous range compared to an equivalent single-output system. This approach will be referred to as I-OFDM in the following.

Due to the high achievable throughput and efficiency, in communication systems, parallel transmission within the same band is often realized via CDM and orthogonal codes. Yet, in MIMO radar systems, utilizing coding for channel separation is not prevalent as self-interference due to imperfect code cross-correlation properties decreases the detection performance of the system [11]. For optimal radar performance, the transmitted signals should have thumbtack-like auto-correlation peaks with a low side-lobe level. Ideally, their auto-correlation function (ACF) is maximum at zero-delay and zero elsewhere. Additionally, to achieve orthogonality and thereby perfect isolation between different transmitters, the cross-correlation function (CCF) of two signals should be zero for all delays. While FDM and TDM naturally offer perfect CCF properties by avoiding signal overlap in time-frequency domain at cost of a reduced coverage in time or frequency and thus emerging ambiguities, CDM must achieve orthogonality in the code dimension. Unfortunately, perfectly orthogonal codes do not exist as the Welch bound shows [12], which gives a theoretical lower bound on the correlation of two signals. Therefore, for good coded MIMO radar operation, waveforms are desired that offer a good trade-off between radar performance and signal isolation. Since OFDM radar waveforms allow for flexible digital signal design and, in addition, phase coding is typically already implemented in the time-frequency domain, they offer optimal conditions for coded MIMO operation.

In this paper, three novel strategies to design coded MIMO OFDM radar waveforms are proposed, compared, and evaluated. The approaches pursue completely different coding strategies, where each of them is adapted for OFDM radar to take advantage of the muli-carrier scheme and digital signal design and processing. The first approach simply uses orthogonal code sets, the second approach aims to eliminate crosstalk by using time-shifted signals, and finally, the third approach combines repeated symbols OFDM (RS-OFDM) with space-time coding (STC). To our best knowledge, these coded MIMO OFDM approaches are presented here for the first time. Additionally, it will be shown that these approaches can achieve a comparable or better performance and thus constitute an alternative to I-OFDM although – by its very nature – it achieves a perfect CCF, which is hardly achievable for coded strategies. It will also be discussed and analyzed at which costs these improvements are achievable.

The paper is organized as follows. The general generation

C. Knill, B. Schweizer, S. Stephany, and C. Waldschmidt are with the Institute of Microwave Engineering, Ulm University, 89081 Ulm, Germany e-mail: christina.knill@uni-ulm.de.

This work was supported in part by the Ministerium für Wissenschaft, Forschung und Kunst (MWK) Baden-Württemberg within the Tech Center a-drive under grant 32-7533-4-10/13/20 and in part by the German Federal Ministry of Education and Research under grant 16EMO0345 (IMIKO-Radar).

of MIMO OFDM radar signals and processing is introduced in Section II, and the influence of cross-channel interference on the range evaluation is derived in Section III. In Section IV, three coded MIMO OFDM strategies are introduced and detailed. An evaluation and comparison of these approaches using simulations and measurements is given in Section V. Finally, in Section V-E, an approach to overcome the maximum unambiguous range limitations for the second strategy is validated using measurements of an approaching vehicle.

II. MIMO OFDM Radar Signals

A standard OFDM frame consists of N subcarriers with spacing Δf and M symbols of duration $T{=}1/\Delta f$. Given K transmit antennas, the OFDM baseband transmit signal of the mth OFDM symbol of the kth transmitter is defined by

$$x_m^{(k)}(t) = \sum_{n=0}^{N-1} d_{mn}^{(k)} \mathrm{e}^{\mathrm{j}2\pi n\Delta f t}\, \mathrm{rect}\left(\frac{t - mT_{\mathrm{OFDM}}}{T_{\mathrm{OFDM}}}\right) \tag{1}$$

where $d_{mn}^{(k)}$ is the modulation symbol of the mth symbol on the nth subcarrier of the kth transmitter, each drawn independently from a modulation alphabet $\mathcal{A}$, e.g., QPSK. To avoid inter-symbol interference (ISI) at the receiver due to path delays, each OFDM symbol is extended by a cyclic prefix (CP) of duration T_{cp} that increases the OFDM symbol duration to $T_{\mathrm{OFDM}}{=}T{+}T_{\mathrm{cp}}$. Finally, for transmission, the baseband signals are converted to the carrier frequency f_c.

Given L receive antennas, the baseband receive signal at the lth receive antenna is a superposition of the simultaneously transmitted signals reflected by P targets. As these reflections are additive in the signal, the number of targets is assumed to be one and the index p will be neglected. The paths between all transmit and receive elements are referred to as *channels* further on. Moreover, a signal transmitted from the kth transmitter and received by the lth receiver will be indicated by the superscript (k,l), whereas the sum of all impinging signals on the lth receiver is indicated by the superscript (l). The baseband receive signal at the lth receiver for the mth symbol then is

$$\begin{aligned} y_m^{(l)}(t) = \sum_{\xi=1}^{K} \sum_{n=0}^{N-1} d_{mn}^{(\xi)} \mathrm{e}^{-\mathrm{j}2\pi(n\Delta f + f_c)\tau^{(\xi,l)}} \mathrm{e}^{\mathrm{j}2\pi f_d t} \mathrm{e}^{\mathrm{j}2\pi n\Delta f t} \\ \times \mathrm{rect}\left(\frac{t - mT_{\mathrm{OFDM}}}{T_{\mathrm{OFDM}}}\right), \end{aligned} \tag{2}$$

where $\tau^{(\xi,l)}{=}R^{(\xi,l)}/c$ and f_d are the delay and Doppler shift of the target reflection in the (ξ,l)th channel, respectively, with target distance $R^{(\xi,l)}$ and c the speed of light. The attenuation in the channel is assumed as a constant and is therefore neglected. Assuming point targets in the far field of the combined transmit and receive aperture and $f_c \gg N\Delta f$ (narrowband assumption), f_d is considered constant for all channels and subcarriers in (2). At the receiver, the baseband signal (2) is Nyquist-sampled, the CP is discarded, and a discrete Fourier transform (DFT) is applied along each OFDM symbol. If the resulting Fourier coefficients of each OFDM symbol are arranged consecutively in a matrix, the $M{\times}N$ receive frame matrix $\boldsymbol{Y}^{(l)}$ with elements

$$Y_{mn}^{(l)} = \sum_{\xi=1}^{K} d_{mn}^{(\xi)} \mathrm{e}^{-\mathrm{j}2\pi(n\Delta f + f_c)\tau^{(\xi,l)}} \mathrm{e}^{\mathrm{j}2\pi f_d m T_{\mathrm{OFDM}}} \tag{3}$$

is obtained. It is assumed that $f_d \ll \Delta f$ [5], [8] such that the effect of inter-carrier interference (ICI) is negligible and is therefore omitted in the signal description. Next the (k,l)th channel is extracted from (3) by element-wise multiplication with the inverse of the transmit modulation symbols $d_{mn}^{(k)}$. Assuming the utilized modulation symbols from $\mathcal{A}$ have unitary amplitudes, e.g., (Q)PSK, this equals the multiplication with the complex conjugate such that the (k,l)th channel extracted from (2) is

$$Y_{mn}^{(k,l)} = \sum_{\xi=1}^{K} d_{mn}^{(\xi)} \left(d_{mn}^{(k)}\right)^{*} \mathrm{e}^{-\mathrm{j}2\pi(n\Delta f + f_c)\tau^{(\xi,l)}} \mathrm{e}^{\mathrm{j}2\pi f_d m T_{\mathrm{OFDM}}}, \tag{4}$$

where the superscript $*$ denotes the complex conjugate. The signal may be further split into two additive parts, the desired part ($\xi = k$)

$$\hat{Y}_{mn}^{(k,l)} = \mathrm{e}^{-\mathrm{j}2\pi(n\Delta f + f_c)\tau^{(k,l)}} \mathrm{e}^{\mathrm{j}2\pi f_d m T_{\mathrm{OFDM}}} \tag{5}$$

and the additive cross-talk part[1] ($\xi \neq k$)

$$\tilde{Y}_{mn}^{(k,l)} = \sum_{\substack{\xi=1 \\ \xi\neq k}}^{K} d_{mn}^{(\xi)} \left(d_{mn}^{(k)}\right)^{*} \mathrm{e}^{-\mathrm{j}2\pi(n\Delta f + f_c)\tau^{(\xi,l)}} \mathrm{e}^{\mathrm{j}2\pi f_d m T_{\mathrm{OFDM}}}, \tag{6}$$

that accounts for the cross-talk due to the activity of other transmitters on the same subcarrier at the same time. In this step, the difference between CDM and F/TDM becomes obvious. For both TDM and FDM only one transmitter is allowed to be active at a certain time (m) and frequency (n) slot such that only NM/K modulation symbols $d_{mn}^{(k)}$ of the frame of the (k,l)th channel are non-zero. In the signal evaluation, this results in

$$\text{F/TDM:} \quad d_{mn}^{(\xi)} \left(d_{mn}^{(k)}\right)^{*} = \begin{cases} 1, & \text{if } \xi = k \text{ and } d_{mn}^{(k)} \neq 0 \\ 0, & \text{if } \xi \neq k \text{ or } \; d_{mn}^{(k)} = 0 \end{cases} \tag{7}$$

since always either $d_{mn}^{(\xi)}$ or $d_{mn}^{(k)}$ is zero. In contrast, for CDM, in general, every transmitter is active the whole time such that

$$\text{CDM:} \quad d_{mn}^{(\xi)} \left(d_{mn}^{(k)}\right)^{*} \neq 0, \qquad \forall k,\xi = 1,\ldots,K\ . \tag{8}$$

Consequently, for F/TDM, the additive cross-talk (6) is always zero but also the desired part (5) becomes zero if the kth transmitter was inactive at slot (m,n). For CDM, both are non-zero in general.

To achieve low inter-transmitter cross-talk for CDM and thereby good channel isolation, the interfering term (6) should be ideally zero for all slots (m,n). Due to (8), this is not possible. Therefore, the goal will be to minimize the influence of (6) on the range-Doppler and range-azimuth evaluation and thereby the target detection. Range-Doppler evaluation for OFDM is commonly achieved by a DFT along the OFDM

[1] In case of non-zero Doppler shifts, (5) contains additional multiplicative cross-talk from other subcarriers in the form of ICI.

symbols (Doppler) and an inverse DFT (IDFT) along the subcarrier dimension (range) of $\boldsymbol{Y}^{(k,l)}$ with elements (4) which yields the range-velocity radar image (R-v-image). For sidelobe suppression, tapering is usually applied in both dimensions before evaluation.

III. Influence of Coded MIMO Signals on the Range Evaluation

Since the IDFT is a linear operation, the resulting *range profiles* $\mathcal{R}_m^{(k,l)}[\rho]$ may again be divided into a desired part $\hat{\mathcal{R}}_m^{(k,l)}[\rho]$ and an interference part $\tilde{\mathcal{R}}_m^{(k,l)}[\rho]$, similar to (5) and (6), where $\rho\in\mathbb{Z}$ is the range bin index and $[\bullet]$ denotes discrete values.

Given the distance of the target to the reference antenna R_0, the time delay in (2) to (6) is composed of

$$\tau^{(k,l)} = \frac{R^{(k,l)}}{c} = \frac{1}{c}\left(2R_0 + \Delta R^{(k)} + \Delta R^{(l)}\right) \tag{9}$$

with corresponding transmit and receive path differences, respectively, of

$$\Delta R^{(k)} = a^{(k)}\sin\theta^{(k)} \quad \text{and} \quad \Delta R^{(l)} = a^{(l)}\sin\theta^{(l)}\ . \tag{10}$$

Here, $a^{(k)}$ and $a^{(l)}$ are the spacings of the kth and lth antenna to the reference antenna, and $\theta^{(k)}$ and $\theta^{(l)}$ are the target angles observed by the transmit and receive antenna, respectively. Due to the far field condition, we suppose $\theta{=}\theta^{(k)}{=}\theta^{(l)}$. Hence, the delay (9) becomes

$$\tau^{(k,l)} = \frac{1}{c}\left(2R_0 + a^{(k,l)}\sin\theta\right) \tag{11}$$

with $a^{(k,l)}{=}a^{(k)}{+}a^{(l)}$. Inserting (11) into (5) and performing the range IDFT, the desired range profile yields

$$\hat{\mathcal{R}}_m^{(k,l)}[\rho] \propto N g\big[\rho-\rho_0\big] \tag{12}$$

with target at range bin $\rho_0{=}\mathrm{round}\big[N\Delta f/c\big(2R_0{+}a^{(k,l)}\sin\theta\big)\big]$ and $g[\rho]$ the peak shape function depending on the applied tapering prior to the IDFT. Here, $\mathrm{round}[\bullet]$ indicates rounding to the nearest integer.

Inserting (11) into (6) and applying the IDFT gives the interference term

$$\tilde{\mathcal{R}}_m^{(k,l)}[\rho] \propto \sum_{n=0}^{N-1}\sum_{\substack{\xi=1\\ \xi\neq k}}^{K-1} \gamma^{(\xi,l)} d_{mn}^{(\xi)}\big(d_{mn}^{(k)}\big)^{*}\mathrm{e}^{\mathrm{j}2\pi\frac{n}{N}(\rho-\rho_0)}\ , \tag{13}$$

where $\gamma^{(\xi,l)}{=}\exp\left(-\mathrm{j}2\pi f_c a^{(\xi,l)}\sin\theta/c\right)$ is a channel dependent constant. Using the discrete time representation of the baseband transmit signal (1) yields that

$$d_{mn}^{(\xi)} = \sum_{\mu=0}^{N-1} x_m^{(\xi)}[\mu]\mathrm{e}^{-\mathrm{j}2\pi\frac{n\mu}{N}} \quad \text{and} \tag{14}$$

$$\big(d_{mn}^{(k)}\big)^{*} = \sum_{\eta=0}^{N-1}\big(x_m^{(k)}[\eta]\big)^{*}\mathrm{e}^{\mathrm{j}2\pi\frac{n\eta}{N}}\ . \tag{15}$$

After rearranging of terms and sums, (13) becomes

$$\begin{aligned}\tilde{\mathcal{R}}_m^{(k,l)}[\rho] \propto \sum_{\substack{\xi=1\\ \xi\neq k}}^{K-1}\gamma^{(\xi,l)}\sum_{\mu=0}^{N-1}\sum_{\eta=0}^{N-1} x_m^{(\xi)}[\mu]\big(x_m^{(k)}[\eta]\big)^{*}\\ \times\underbrace{\sum_{n=0}^{N-1}\mathrm{e}^{\mathrm{j}2\pi\frac{n}{N}(\rho-\rho_0-\mu+\eta)}}_{\alpha}\ .\end{aligned} \tag{16}$$

Here α is only non-zero (and equals N) if the phases of the exponential function become zero, e.g., if $\mu=\big[\rho-\rho_0+\eta\big]_N$ where $[\bullet]_N$ indicates the modulo N operation. Through this, (16) finally becomes

$$\tilde{\mathcal{R}}_m^{(k,l)}[\rho] \propto \sum_{\substack{\xi=1\\ \xi\neq k}}^{K-1}\gamma^{(\xi,l)}\underbrace{\sum_{\eta=0}^{N-1} x_m^{(\xi)}[\eta+\rho-\rho_0]_N\big(x_m^{(k)}[\eta]\big)^{*}}_{\text{periodic CCF shifted by }\rho_0}, \tag{17}$$

where the last sum equals the periodic CCFs of the sampled time-domain transmit signals with respect to the kth transmitter. Moreover, the CCF is also shifted by the target position due to the signal delay. Hence, to reduce the influence of the interfering term, the CCFs of the sampled time-domain signals must be minimized.

IV. Coded MIMO Approaches with optimized Channel Isolation

According to the Welch bound, it is impossible to obtain both perfect ACF and CCF and thereby perfect channel isolation in CDM. The Welch bound is a theoretical limit of the achievable isolation of two distinct codes of length $\mathcal{L}$ that are taken from a common code set of cardinality $\mathcal{M}$. It is defined as

$$w = \sqrt{\frac{\mathcal{M}-1}{\mathcal{M}\mathcal{L}-1}} \tag{18}$$

where for sets with $\mathcal{M}\to\infty$, the bound is approximated with $w(\mathcal{M}\to\infty)\approx\sqrt{1/\mathcal{L}}$. To illustrate its importance for radar, suppose a naive CDM MIMO OFDM approach of using two sequences with $N{=}\mathcal{L}{=}1024$ symbols independently drawn from the QPSK alphabet. The correlation result at the receiver is then the superposition of the ACF and CCF where the sidelobe level is defined by the CCF and the main lobe by the ACF, as shown in Fig. 1. With member size $\mathcal{M}{=}N^4$, the Welch bound only yields $w^{\text{naive}}{\approx}{-}30\,\mathrm{dB}$ as achievable isolation. By doubling or quadrupling the number of interfering transmitters, the isolation at the receiver is further reduced by $3\,\mathrm{dB}$ and $6\,\mathrm{dB}$, respectively, due to the multiple signal superposition. Therefore, in radar applications this approach would lead to high self-interference, which would severely degrade the system performance. Moreover, the application of sophisticated codes such as maximum length sequences (MLS), Gold codes, or almost perfect auto-correlation sequences (APAS) are also not advantageous as these codes are designed for good ACF but suffer from moderate CCF properties in the range of the Welch bound [13].

Yet, though it seems impossible to achieve perfect isolation for the complete frame, it is possible to achieve perfect isolation, e.g., for a limited region. In the following, three

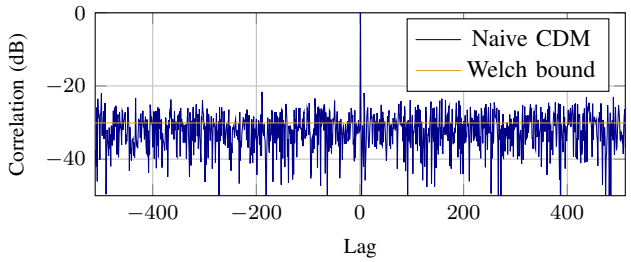

Fig. 1. Naive CDM MIMO OFDM example. Correlation result of two random QPSK code sequences of length 1024 and the corresponding Welch bound.

coded MIMO OFDM strategies are presented that achieve almost optimal channel isolation under some constraints.

A. Zero-Correlation Zone CDM (ZCZ-CDM)

Zero-Correlation Zone (ZCZ) code sets have optimal ACF and CCF up to a certain delay. In asynchronous or approximately synchronized CDMA communication systems, ZCZ code sequences are used, e.g., for synchronization purpose or to reduce the co-channel interference [14], [15]. In radar, ZCZ codes have also been investigated for phase-coded CW MIMO radars [16] or PMCW MIMO radars [13]. Commonly, a ZCZ sequence set $\mathcal{C}$ is described by the tuple $(\mathcal{L},\mathcal{M},\mathcal{Z})$, where $\mathcal{L}$ is the length of each sequence in the set, $\mathcal{M}$=$\{\mathcal{C}\}$ the cardinality of the set, and $\mathcal{Z}$ the width of the ZCZ. In [15], it is shown that there is a theoretical upper bound on $\mathcal{Z}$ of $\mathcal{Z}_{\text{opt}}$=$\mathcal{L}/\mathcal{M}-1$ which is derived from the Welch bound.

In order to take advantage of the ZCZ property in coded MIMO OFDM, the ZCZ code needs to be applied in time-domain. To this end, it is convenient to take a PMCW-like point of view of the transmit signal while maintaining the OFDM processing chain. The following steps are applied OFDM-symbol-wise. First, K codes $\{c_m^{(k)}[\eta]\}_{\eta=0,\dots,\mathcal{L}-1}$, k=$1,\dots,K$ from $\mathcal{C}$ are chosen randomly and assigned to the transmitters. Hence, for unique signals on every transmitter the cardinality $\mathcal{M}$ must be at least K. Next, the corresponding frequency domain modulation symbols

$$d_{mn}^{(k)} = \sum_{\eta=0}^{N-1} c_m^{(k)}[\eta]\mathrm{e}^{-\mathrm{j}2\pi\frac{n\eta}{N}} \tag{19}$$

are computed using a DFT of length N. The code length should therefore be $\mathcal{L}$=N.

As the ZCZ codes are applied in time-domain, i.e., $x_m^{(k)}[\eta]$=$c_m^{(k)}[\eta]$, the resulting actually applied modulation symbols (19) have non-uniform amplitudes and arbitrary phases such that the unitary amplitudes alphabet constraint assumed for (4) is violated. Yet, the codes have the peculiarity that their periodic CCF $\Psi_{k\xi}[\rho]$=$\sum_{\eta=0}^{N-1} x^{(\xi)}[\eta+\rho]_N\big(x^{(k)}[\eta]\big)^*$ disappears for $\rho\leq\mathcal{Z}$ [14], [15]. For coded OFDM this cancellation is induced in the range processing in (17) but only if the multiplication with the complex conjugate is applied in (4) despite of non-uniform amplitudes. Otherwise, a similarly poor result as in Fig. 1 will be obtained.

For ZCZ-CDM OFDM radar operation, the ZCZ sequence set construction from [14] is adopted in the following. In this case, a QPSK ZCZ sequence set is constructed from complex recursively interleaved Hadamard matrices. The resulting sequence sets are given by the tuple $\mathcal{C}$=$(\mathcal{L},\mathcal{M},\mathcal{Z})$=$(2^{i+2}q, 4q, 2^{i-2}3)$ where the parameter $q\geq1$ is the order of the initial Hadamard matrix before the first recursive interleaving step and $i\geq0$ is the interleaving or recursion depth required to obtain the desired code length $\mathcal{L}$. Note that any such set achieves a ZCZ length of $\mathcal{Z}\approx3/4\mathcal{Z}_{\text{opt}}$. Next, it will be briefly derived how to optimally choose q and i given N and K of the OFDM radar. For details on the code generation procedure, the reader is referred to [14]. For an OFDM system with K transmitters, the number of sequences in the set has to be $\mathcal{M}$=$4q\geq K$. Given K' is the smallest integer $K'\geq K$ such that $(K' \mod 4)$=0, the relation becomes q=$K'/4$. Additionally, the code length should equal the number of subcarriers which gives N=$2^{i+2}q$. With the tuning of q, the expression is solved after variable i which gives the recursion depth i=$\log_2(N/K')$. Finally, the ZCZ becomes $\mathcal{Z}$=$3N/(4K')$ which supports the claim that K' should be as small as possible in order to maximize $\mathcal{Z}$.

B. Auto-Correlation-Based CDM (AC-CDM)

If two distinct transmitters would both emit the same signal, the desired range term (12) and the interference term (17) would become equal, and the interference disappears as the periodic CCF in (17) then becomes a periodic ACF as in (12). Yet, the signals would not be distinguishable at the receiver anymore and it seems as if the signal comes from a single transmitter. In auto-correlation-based CDM (AC-CDM), it is proposed to transmit identical signals in a seemingly time-delayed fashion in order to be able to separate them at the receiver again. This idea is comparable with the time-staggered MIMO [3], [7]. However, asynchronous transmission on multiple antennas leads to phase shifts between different channels at the receiver, which complicates the direction of arrival (DoA) estimation. Fortunately, for OFDM it is possible to only virtually delay the signals by rotating them circularly within one OFDM symbol by the desired delay. Thereby, no offset between the channels is generated and the OFDM symbols are synchronous at both transmitter and receiver.

Define the relative mutual (sample) shift $s^{(k\xi)}$ between the ξth and the kth transmitter to be $-N/2\leq s^{(k\xi)}\leq N/2$. The virtual signal delay becomes $s^{(k\xi)}\delta_t\in[-T/2, T/2]$ with sample duration δ_t=T/N. In order to be able to separate the transmitters at the receiver, the mutual delays must be $|s^{(k\xi)}|>0$, $\forall k\neq\xi$. The transmit signals with respect to the kth transmitter are then given by

$$x_m^{(\xi)}(t) = x_m^{(k)}\big((t - s^{(k\xi)}\delta_t)_T\big), \quad \forall\xi = 1,\dots,K, \tag{20}$$

where $(\bullet)_T$ denotes the modulo T operation. Conveniently, these signals may be directly generated digitally within the standard OFDM processing by simply adjusting the OFDM frequency modulation symbols $d_{mn}^{(k)}$. In this case, the modulation symbols $d_{mn}^{(k)}$ may take any phase. Define any reference antenna k, whose modulation symbols $d_{mn}^{(k)}$ are drawn randomly from the modulation alphabet. Using the Fourier

relation $x(t-\Delta t) \circ\!\!-\!\!\bullet\, X(f)\exp(-\mathrm{j}2\pi\Delta t f)$, the resulting modulation symbols of antenna ξ are

$$d_{mn}^{(\xi)} = d_{mn}^{(k)} \mathrm{e}^{-\mathrm{j}2\pi s^{(k\xi)}\delta_t n\Delta f} \quad , \quad \forall \xi = 1,\dots,K \ . \tag{21}$$

Inserting (20) into (17), the discrete periodic CCF will become a periodically shifted ACF of $x_m^{(k)}$ according to

$$\begin{aligned}\tilde{\mathcal{R}}_m^{(k,l)}[\rho] &\propto \sum_{\substack{\xi=1\\ \xi\neq k}}^{K-1} \gamma^{(\xi,l)} \sum_{\eta=0}^{N-1} x_m^{(k)}[\eta+\rho-\rho_0 - s^{(k\xi)}]_N \big(x_m^{(k)}[\eta]\big)^* \\ &\propto \sum_{\substack{\xi=1\\ \xi\neq k}}^{K-1} \gamma^{(\xi,l)} g\big[\rho-\rho_0-s^{(k\xi)}\big] \ , \end{aligned} \tag{22}$$

with shift of $\rho_0+s^{(k\xi)}$ per transmitter ξ. Just as the ACF in (12), each of these shifted ACFs will result in a peak in the radar image of the kth channel such that in total K peaks per target emerge: One peak through the ACF in (12) at the correct range bin at ρ_0 and $K-1$ ambiguous peaks at bins $\rho_0+s^{(k\xi)}$ caused by the shifted ACFs of the interfering channels in (22).

Though this seems very unfavorable, by introducing simple modifications and smart signal processing, the same unambiguous range as in the SISO case is achievable despite the inevitably arising ambiguities.

1) Choice of Mutual Shifts: By obeying the following constraints, a favorable choice of mutual shifts is obtained:

(I) Each mutual shift $s^{(k\xi)}$, $\xi \neq k$, should be unique where the difference between any two mutual shifts should be at least N_{guard}. Through this, the peaks from (22) become separable and unique in the common radar image of all channels.

(II) N_{guard} should be at least the minimum distance between two targets required to be distinguishable in the detection step. Typically, this depends on the tapering and is in the range of 3 to 10 bins.

(III) In each channel, the distance between any target's main peak and its ambiguous peaks should be maximized.

Through this, the minimum number of bins between the main and the closest ambiguity peak of one channel is

$$N_{\text{ua}}^{\text{AC}} = \left\lfloor \frac{N}{K} - \frac{N_{\text{guard}}(K+1)}{2} \right\rfloor \tag{23}$$

and the mutual shifts are

$$s^{(k\xi)} = (\xi-k)N_{\text{ua}}^{\text{AC}} + \frac{\xi(\xi-1)-k(k-1)}{2} N_{\text{guard}} \ , \tag{24}$$

where $(k,\xi)\epsilon[1,K]$. This guarantees that constraints (I) and (III) are fulfilled but constraint (II) might be violated for few mutual shifts as the modulo operation was neglected for simplicity. Yet, this is tolerable. In Table I, an example design for the mutual shifts with K=4, N=1024, and N_{guard}=7 is given. Note that for N_{guard}=0, the range profiles become similar to those of I-OFDM.

2) Resolving Ambiguities: As described in Section III, the range profile of the (k,l)th channel is composed of the desired part (12), which gives a target peak at ρ_0, and the interference part (22), which gives further peaks at $\rho_0+s^{(k\xi)}$ for AC-CDM. This sums up to K peaks per target where always one of these peaks is at the correct range bin ρ_0 and the remaining are ambiguous and are not distinguishable from the correct one given a single channel only. However, through the design rule (24), which creates pairwise different shifts between the transmitters ξ and k, the ambiguous target at $\rho_0+s^{(k\xi)}$ in the (ξ,l)th channel becomes unique among all channels of the lth receiver as $s^{(k\xi)}$ is unique. This is illustrated in the example shown in Table I and Fig. 2 where the figure shows the range profiles of the K channels of any receiver l for a scene with a single target at range bin ρ_0. As the mutual shifts between any two channels is unique, only the target at its correct position ρ_0 is common in all channels, while its ambiguities are unique across all channels. Therefore, correct target peaks can be recognized by the fact that they are present in the same range bin in each channel, whereas ambiguous peaks are unique across all channels. AC-CDM with ambiguity detection will be indicated with AC$^+$-CDM in the following.

TABLE I
AC-CDM MUTUAL SHIFTS $s^{(k\xi)}$ EXAMPLE FOR K=4, N=1024, AND N_{GUARD}=7 USING (24).

ξ \ k	1	2	3	4
1	0	−245	−497	268
2	245	0	−252	−511
3	497	252	0	−259
4	−268	511	259	0

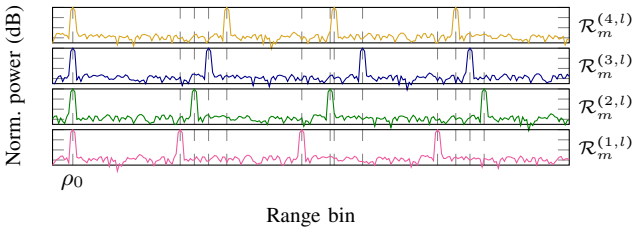

Fig. 2. Illustration of an exemplarily ambiguities distribution in AC-CDM across the channels of a single receiver l for a system with four transmitters and a single target at ρ_0.

C. Modified Repeated Symbols MIMO (MRS-CDM)

In modified repeated symbol CDM (MRS-CDM), repeated symbol (RS) OFDM [17] is combined with space-time coding (STC) [11]. RS-OFDM uses the same modulation symbol on each subcarrier for the complete radar frame. Similar to [11], the idea in MRS is to cancel the CCF by accumulating consecutive, properly coded, OFDM symbols. The accumulation is already included in the OFDM evaluation within the Doppler evaluation and thus does not represent a modification of the usual processing. MRS is related to Hadamard coding MIMO waveform in [3] or short-time CDM [18] for FMCW radars and outer coding MIMO PMCW [7]. As in [11], STC will be implemented using a Hadamard matrix H_K of order K where

$$H_2 = \begin{bmatrix} 1 & 1 \\ 1 & -1 \end{bmatrix}, \quad \text{and} \quad H_K = \begin{bmatrix} H_{K/2} & H_{K/2} \\ H_{K/2} & -H_{K/2} \end{bmatrix} . \tag{25}$$

Hadamard matrices have the property that the Euclidean norm of each row or column is K and the inner product of distinct rows or columns is zero. In the proposed approach, the first property yields an ideal ACF where the second property eliminates the cross-talk.

The coding is done blockwise for each subcarrier, where a block involves all K transmitters (*space*, rows of (25)) and K consecutive symbols (*time*, columns of (25)). These blocks are repeated until M symbols are obtained. To this end, K modulation symbols s_k are randomly chosen from $\mathcal{A}$. Then the STC via (25) is applied where in the assignment also permutations are allowed. E.g., for K=2, four conceivable designs are

$$S_1 = \begin{matrix} m & m{+}1 \\ \end{matrix} \begin{matrix} \\ \end{matrix} \begin{bmatrix} s_1 & s_1 \\ s_2 & -s_2 \end{bmatrix} \begin{matrix} \text{TX 1} \\ \text{TX 2} \end{matrix}, \quad S_2 = \begin{matrix} m & m{+}1 \\ \end{matrix} \begin{matrix} \\ \end{matrix} \begin{bmatrix} s_1 & s_2 \\ s_2 & -s_1 \end{bmatrix} \begin{matrix} \text{TX 1} \\ \text{TX 2} \end{matrix}$$
$$S_3 = \begin{matrix} m & m{+}1 \\ \end{matrix} \begin{matrix} \\ \end{matrix} \begin{bmatrix} s_1 & -s_1 \\ s_2 & s_2 \end{bmatrix} \begin{matrix} \text{TX 1} \\ \text{TX 2} \end{matrix}, \quad S_4 = \begin{matrix} m & m{+}1 \\ \end{matrix} \begin{matrix} \\ \end{matrix} \begin{bmatrix} s_1 & s_1 \\ -s_2 & s_2 \end{bmatrix} \begin{matrix} \text{TX 1} \\ \text{TX 2} \end{matrix} \tag{26}$$

where S_1 constitutes the straightforward design. Beyond this, it is possible to permute the order of the columns or rows of the Hadamard matrix (S_4/S_3) or to permute the assignment of s_k over the transmitters of a single symbol (S_2). The chosen design has to be maintained for this subcarrier until the end of the signal frame, i.e. for M OFDM symbols. However, it is possible to use different assignments for different subcarriers, which introduces more flexibility to the signal design. Note that the utilized block structure (26) is different than for outer-coding MIMO PMCW [7] and by the independent subcarrier design it is not necessarily given that the signal can be translated into an outer-code. For simplicity, in the following, assignment S_1 will be utilized for each subcarrier. The sequences of modulation symbols $\boldsymbol{D}_n^{(k)}$=$[d_{0n}^{(k)}, d_{1n}^{(k)}, \ldots, d_{(M-1)n}^{(k)}]$ of the nth subcarrier then become (K=2)

$$\boldsymbol{D}_n^{(1)} = [s_1, s_1, \ldots, s_1], \quad \boldsymbol{D}_n^{(2)} = [s_2, -s_2, \ldots, s_2, -s_2]. \tag{27}$$

Thereby, the sequences $\boldsymbol{D}_n^{(k)}$ become block-periodic with period K. Each block contains the repetition of the symbol s_k=$d_{0n}^{(k)}$ with alternating sign according to the kth row of S. The remaining signal generation is identical to the conventional approach. Note that other than in RS-OFDM, where the CP can be omitted, a CP is required in MRS-CDM due to the introduced phase shifts.

For evaluation, the common processing chain as described in Sections II and III is applied. The velocity DFT is of particular importance for MRS-CDM: it is only through this step that the transmitters finally become orthogonal as the summation in the DFT eliminates the cross-talk. Similar to the range evaluation, the resulting Doppler profile $\mathcal{V}_n^{(k,l)}[\nu]$ of the nth subcarrier of the (k,l)th channel may be divided into a desired part $\hat{\mathcal{V}}_n^{(k,l)}[\nu]$ and an interference part $\tilde{\mathcal{V}}_n^{(k,l)}[\nu]$.

The Doppler DFT of (5) gives the desired part

$$\hat{\mathcal{V}}_n^{(k,l)}[\nu] \propto M g\big[\nu - \nu_0\big], \tag{28}$$

TABLE II
OFDM SIGNAL PROPERTIES.

Parameter	Symbol	Value
Subcarriers	N	1024
Symbols/frame	M	2048
Subcarrier spacing	Δf	400 kHz
OFDM symbol duration	T	2.5 µs
Bandwidth	B	409.6 MHz
Carrier frequency	f_c	77 GHz
Cyclic prefix duration	T_{cp}	0.4 µs
Range resolution	Δr	36.6 cm
Velocity resolution	Δv	0.3 m/s

that yields a target peak at ν_0=round$[f_d M T_{\text{OFDM}}]$. The DFT of (6) yields, after inserting (27) and applying further simplifications,

$$\tilde{\mathcal{V}}_n^{(k,l)}[\nu] \propto \frac{M}{K}\, g\big[\nu - \nu_0\big]_{\frac{M}{K}} \sum_{\substack{\xi=1 \\ \xi\neq k}}^{K-1} \Gamma^{(\xi,l)} d_{0n}^{(\xi)} \left(d_{0n}^{(k)}\right)^* \times \sum_{u=1}^{K} h_{\xi u} h_{ku} \mathrm{e}^{\mathrm{j}2\pi \frac{u-1}{M}(\nu_0-\nu)} \tag{29}$$

where $\Gamma^{(\xi,l)}$=$\exp\{\mathrm{j}2\pi n \Delta f \tau^{(k,l)}\}$ assuming that the range IDFT was not yet applied and h_{ku} being the element of the kth row and uth column of (26). It shows that the interference part exhibits peaks at ν=$\nu_0 + \kappa M/K$, κ=$1, \ldots, (K-1)$ with periodicity M/K. Note that the target at ν=ν_0 is missing as in this case the last sum equals the inner product of two columns of the Hadamard matrix which is zero.

It should be noted that MRS should not be applied in the range dimension, i.e. along the subcarriers. The reason is that in this case the signal would become a so-called uncoded OFDM, as every subcarrier of an OFDM symbol would be coded with the same phase. However, this leads to a pulse-like time-domain signal with high amplitude fluctuations which is unfavorable for amplification using linear power amplifiers.

V. COMPARISON AND EVALUATION USING SIMULATIONS AND MEASUREMENTS

Different properties and the performance of the proposed coded MIMO OFDM strategies are now analyzed and compared. We restrict ourselves to the quantities for which significant differences were expected and observed in simulations and measurements. These are the achievable maximum unambiguous regions, the Doppler sensitivity, and the achievable peak-to-noise ratio (PNR). At the end of this section, the findings of all evaluations are summarized and application examples are given.

A. Signal Properties and Measurement Setup

For both simulations and measurements, the same signal properties are applied. The general OFDM parameters are listed in Table II. The number of transmitters is K=4 and the number of receivers is L=4 yielding a 4×4 MIMO setup. For each approach the transmit time-domain signals are generated according to Section IV with the following specifications:

- The ZCZ code set is $\mathcal{C}_{\text{ZCZ}}^{(4)}$=$(1024, 4, 192)$.
- For AC-CDM the number of guard bins is N_{guard}=7. Using (24) gives the set of mutual shifts in Table I.
- For MRS-CDM, Hadamard matrices of order 4 are used.

As comparison, an I-OFDM signal with four times interleaving is used. The experimental radar used for the presented measurements has an antenna array with four transmit and four receive channels. Its virtual array is a uniform linear array (ULA) of spacing $\lambda/2$ with 16 elements total. To generate the baseband transmit signal and store the baseband receive signals, a Xilinx RFSoC [19] is used. The signal evaluation is performed offline in MATLAB. For tapering in the 2D-(I)DFT range-Doppler evaluation, Hann-windows are applied in both dimensions.

B. Maximum Unambiguous Regions

The *maximum unambiguous range* R_{ua} achievable for an OFDM radar signal is generally defined by

$$R_{\text{ua}} = N_{\text{period}}\Delta r \quad \leq \quad R_{\text{ua}}^{\max} = cT/2\,, \tag{30}$$

where $N_{\text{period}}{\leq}N$ is the periodicity of the finite IDFT or of the input signal for the range evaluation and $\Delta r{=}c/(2N\Delta f)$ is the range resolution. The maximum periodicity is N which yields the upper bound $R_{\text{ua}}^{\max}$.

The *maximum unambiguous velocity* v_{ua} of an OFDM frame is generally defined by

$$|v_{\text{ua}}| = \frac{M_{\text{period}}}{2}\Delta v \quad \leq \quad |v_{\text{ua}}^{\max}| = \frac{c\Delta f}{4f_c(1+T_{\text{cp}}/T)}\,, \tag{31}$$

where $M_{\text{period}}{\leq}M$ is the periodicity of the velocity DFT or its input signal and $\Delta v{=}c/(2f_cT_{\text{OFDM}}M)$ is the velocity resolution. The maximum periodicity of an OFDM frame is M which yields the upper bound $|v_{\text{ua}}^{\max}|$.

1) Ambiguity Functions: In Fig. 3, the respective characteristic correlation results of the investigated MIMO OFDM signals are shown by means of either the range or velocity ambiguity function. The simulation results are obtained as follows. First all time domain transmit signals (K=4) are summed up to obtain a receive signal corresponding to an ideal single target at R=0 m and v=0 m/s. Next, one channel is extracted as in (4). Finally, the range-Doppler 2D-(I)DFT yields the ambiguity function comprising a superposition of the ACF and $K-1$ CCFs. For I-OFDM, ZCZ-, and AC-CDM, the range profiles at v=0 m/s and for MRS the velocity profile at R=0 m are given. Additionally, the highlighted regions show the theoretical maximum unambiguous range and velocity regions. Ideal isolation is achieved within these unambiguous regions and sharp ambiguity peaks emerge beyond that limit for I-OFDM, AC-, and MRS-CDM. For ZCZ-CDM, an interval of high correlation emerges instead.

2) I-OFDM: The periodicity of the range IDFT is reduced by K due to the interleaving, which resembles a subsampling across the subcarriers such that only every Kth subcarrier is non-zero. Therefore, the unambiguous range reduces to

$$R_{\text{ua}}^{\text{I-OFDM}} = \frac{N}{K}\Delta r\ . \tag{32}$$

In Doppler, no additional ambiguities emerge.

TABLE III
COMPARISON OF MAXIMUM UNAMBIGUOUS RANGES.

	I-OFDM	ZCZ-CDM	AC-CDM*	MRS-CDM
$R_{\text{ua}}/\Delta r$	$\frac{N}{K}$	$\frac{3N}{4K}$	$\left\lfloor \frac{N}{K} - \frac{N_{\text{guard}}(K+1)}{2} \right\rfloor$	N
$v_{\text{ua}}/\Delta v$	M	M	M	$\frac{M}{K}$

* without ambiguity detection

3) ZCZ-CDM: As visualized in Fig. 3b, beyond the ZCZ, intervals of high amplitude emerge. As those ridges in range will not cause distinct targets, they are not considered as ambiguities, however, they should be kept out of the radar's operational range to avoid disturbance. The maximum unambiguous range is therefore limited to the ZCZ. This gives

$$R_{\text{ua}}^{\text{ZCZ}} = \mathcal{Z}\Delta r = \frac{3}{4}\mathcal{Z}_{\text{opt}}\Delta r = \frac{3N}{4K}\Delta r\,, \tag{33}$$

which is $1/K$ less than for I-OFDM. Though, no false targets are generated. In Doppler, no additional ambiguities emerge.

4) AC-CDM: As shifted versions of the same signal are transmitted, ambiguities emerge. Their locations in the individual channels depend on the mutual shifts $s^{(k\xi)}$ of every transmit signal ξ compared to the signal k. According to the proposed constraint signal generation in Section IV-B, the minimum range between the target main peak and its closest ambiguity is proportional to N_{ua} (23) such that

$$R_{\text{ua}}^{\text{AC}} = N_{\text{ua}}\Delta r = \left\lfloor \frac{N}{K} - \frac{N_{\text{guard}}(K+1)}{2} \right\rfloor \Delta r\,, \tag{34}$$

which is $N_{\text{guard}}(K+1)\Delta r/2$ less than for I-OFDM. Note that for AC$^+$-CDM the achievable range is up to $R_{\text{ua}}^{\text{AC+}}$=$R_{\text{ua}}^{\max}$. In Doppler, no additional ambiguities emerge.

5) MRS-CDM: No ambiguities emerge in range such that $R_{\text{ua}}^{\text{MRS}}$=$R_{\text{ua}}^{\max}$. However, unlike the other approaches, ambiguities emerge in Doppler due to the Hadamard matrix coding. The Doppler evaluation yields the superposition of (28) and (29) that together exhibit a periodicity of M/K as derived in Section IV-C. Consequently, the ambiguity-free region is reduced to

$$|v_{\text{ua}}^{\text{MRS}}| = \frac{M}{2K}\Delta v \quad \Leftrightarrow \quad |f_{d,\text{ua}}^{\text{MRS}}| = \frac{\Delta f}{4K(1+T_{\text{cp}}/T)} \tag{35}$$

for the relative velocity and Doppler frequency, respectively.

In order to limit the impact of ICI, a generous excess in Doppler is typically included in the OFDM signal design, but is not used. To this end, a maximum expected Doppler shift $f_{d,\max}$ is defined in the design and the subcarrier spacing of $\Delta f{=}\beta f_{d,\max}$ is deduced where β is typically about 10 [5], [20]. To avoid ambiguities to occur within the expected Doppler range, it must apply $f_{d,\text{ua}}^{\text{MRS}}{\geq}f_{d,\max}$. Thus $\beta{\geq}2K(1+T_{\text{cp}}/T)$ and with $0{\leq}T_{\text{cp}}{\leq}T$, it yields that $2K{\leq}\beta{\leq}4K$ depending on T_{cp}. Consequently, for 2 and 4 transmitters, the typical signal design is sufficient and possible ambiguities are of minor matter. For more transmitters, the subcarrier spacing should be adjusted according to the desired β.

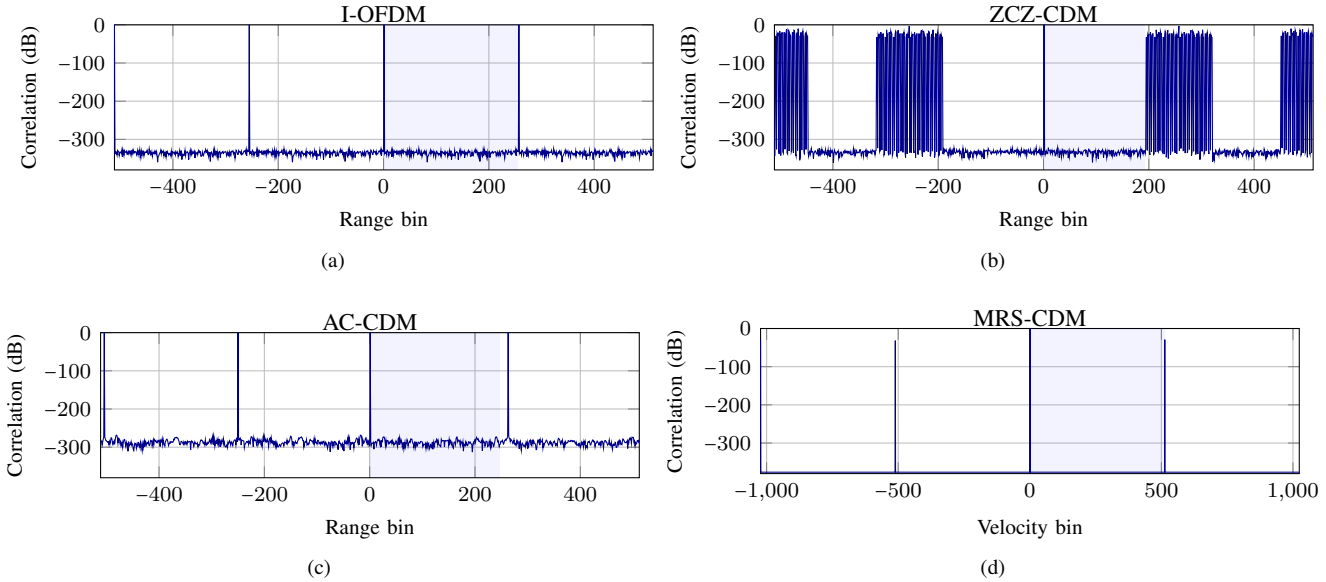

Fig. 3. Correlation results respectively range profiles for (a) I-OFDM, (b) ZCZ-CDM, and (c) AC-CDM, as well as the velocity profile for (d) MRS-CDM. For ZCZ-CDM, the used code sequence set is $\mathcal{C}_{\text{ZCZ}}^{(4)}$=(1024, 4, 192). For AC-CDM, a guard interval of N_{guard}=7 is used. Unambiguous regions are highlighted.

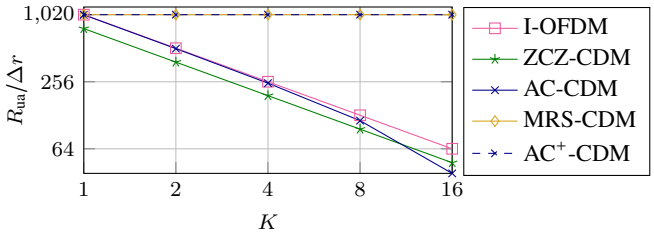

Fig. 4. Comparison of the maximum unambiguous ranges (Table III) for I-OFDM and CDM for different K with N=1024 and N_{guard}=7.

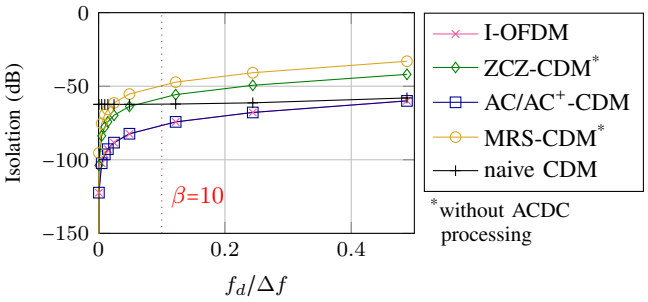

Fig. 5. Doppler sensitivity of I-OFDM, naive CDM, and the proposed CDM MIMO approaches.

TABLE IV
NUMERICAL EXAMPLES FOR R_{UA} AND v_{UA} GIVEN THE OFDM PARAMETERS IN TABLE II FOR K={2, 4, 8, 16} TRANSMITTERS.

	K	I-OFDM	ZCZ	AC	AC⁺	MRS
R_{ua}	2	187.4 m	140.5 m	183.3 m	374.7 m	
	4	93.7 m	70.3 m	87.1 m		
	8	46.8 m	35.1 m	35.1 m		
	16	23.4 m	17.6 m	1.5 m		
v_{ua}	2	335.6 m/s				167.8 m/s
	4					83.9 m/s
	8					42.0 m/s
	16					21.0 m/s

6) Discussion: The achievable maximum unambiguous ranges are summarized in Table III. In Fig. 4, the behavior of R_{ua} for different K is shown. In Table IV, actual values for R_{ua} and v_{ua} given the OFDM parameters in Table II are summarized. In short, it shows that ZCZ-CDM has the lowest operational range though no sharp ambiguous targets are generated. I-OFDM and AC-CDM have similar limitations where the small difference between them will only become obvious for large K. In MRS-CDM R_{ua} is independent of the number of transmitters. The same is achievable for AC⁺-CDM.

In velocity, ambiguities only emerge for MRS due to the Hadamard code structure. Yet, for up to 4 transmitters, the typical safety margin introduced in subcarrier spacing to diminish loss of subcarrier orthogonality allows generous reductions in Doppler ambiguity before the maximum unambiguous region reaches this limit.

C. Doppler and Frequency Offset Sensitivity

OFDM is known to be sensitive to Doppler shifts or frequency offsets [8], [20]. Their presence in the receive signal typically leads to a violation of the subcarrier orthogonality (isolation), which results in reduced target peak power and induced ICI. Both are functions of f_d, where the additional interference constitutes the more prominent degradation.

In Fig. 5, the theoretical isolation in presence of a Doppler shift $f_d/\Delta f$ is shown for I-OFDM and the proposed CDM approaches. I-OFDM and AC-CDM show the same behavior, which also resembles the typical ICI loss for standard OFDM. In naive CDM, the self-induced interference is higher than

the typical Doppler loss (I-OFDM curve) such that ICI loss is not discernible. MRS- and ZCZ-CDM show a significant higher sensitivity to Doppler shifts and ICI than AC-CDM. For ZCZ- and MRS-CDM, the elimination of the cross-talk due to the code dissolves with increasing code compression through the Doppler. In this case, the cross-interference of the other transmit signals will not be completely eliminated. The reduced performance is typical for RS signals or OFDM signals with linearly dependent OFDM symbols. Yet, in [21], it is shown that this circumstance can be exploited to completely reverse the Doppler induced ICI through all-cell Doppler-correction (ACDC) processing. By applying a slightly modified processing scheme, the Doppler shift is compensated before transforming the time domain receive signal to frequency domain[2]. MRS as well as ZCZ-CDM signals are composed of linearly dependent OFDM symbol sequences and are therefore suitable for ACDC processing. After ACDC processing, the same isolation as in Figs. 3b and 3d are obtained for ZCZ and MRS, respectively, independent of the present Doppler shift or number of targets.

D. Achievable Peak-To-Noise Ratio in Measurements

The achievable PNR in the R-v-image is validated using MIMO measurements of a static scenario in an anechoic chamber. The measured static scene is composed of three targets as shown in Fig. 6a. The targets are placed at ranges and angles $(R;\phi)$ of (2.2 m; 26°), (3.7 m; −3°), and (5.7 m; −19.5°) with respect to the reference antenna.

For each measurement a common R-v-image is computed by non-coherent integration of the R-v-images of all 16 channels. Then the achieved PNR is obtained by the ratio of the peak power of the strongest target (R=3.7 m) and the noise level. In Fig. 7, the obtained range profiles (v=0 m/s) of all approaches are shown including the first ambiguity region. Concerning shape and amplitude of the three targets, no difference between the approaches is observable and all peaks are clearly visible and distinguishable. Investigating the noise level starting from R=10 m, for I-OFDM, AC-, and ZCZ-CDM, hardly any differences are observable. However, MRS-CDM shows a slightly reduced PNR.

In Fig. 8, the actually achieved PNRs in dB for the stationary image (range-profile only) and the overall image are compared. Additionally, the ratio of the strongest target to the highest sidelobe, the peak-sidelobe-level (PSLL), is shown. The proposed CDM schemes achieve at least the same PNR as I-OFDM, where ZCZ even achieves an improvement of about 2.5 dB. Concerning the PNR across the range profiles of the targets and the PSLL, the performance of AC is comparable to that of I-OFDM, whereas ZCZ shows both an improvement of the PNR and a decreased PSLL. As already indicated in Fig. 7, MRS shows slightly worse results for both values as it is sensitive to amplitude scaling differences over time or between OFDM symbols, which is likely in the used measurement system. In this case, the CCF interference is not perfectly eliminated and largely concentrates in a ridge along the zero-velocity cut, which is typical for RS-OFDM.

[2]ACDC processing does not constitute an increased effort in processing compared to the standard procedure and is also target scene independent.

E. Resolving Ambiguities in AC-CDM

As already suggested and illustrated in Section IV-B, it is possible to separate ambiguous from correct targets up to $R_{\text{ua}}^{\max}$. In the following, the performance of this procedure is investigated using a more challenging outdoor non-static measurement scenario comprising an approaching vehicle. The radar is placed at about 20 cm above ground and observes the scene from a slanted angle as shown in the photo in Fig. 6b which is taken from the observation angle during measurements. The vehicle is approaching the radar with about v≈30 km/h.

With K=4 transmitter and N_{guard}=7, the maximum unambiguous range in (34) without post-processing yields $R_{\text{ua}}^{\text{AC}}$≈87 m. In the evaluation, the signals of all channels (4) are first extracted and their R-v-image via 2D-(I)DFT processing are computed. The non-coherent integration of all channel images yields the combined radar image as shown in Fig. 9a. Using an ordered-statistic constant false-alarm rate (OS-CFAR) detector, targets are estimated for both the overall image as well as of each channel individually. In Fig. 9a and 10a, the CFAR detections are marked as crosses. Four groups of targets are recognizable. It is noticeable that the targets within these groups are not arranged in the same way, as it would be the case in I-OFDM, where the groups would be exact copies of each other shifted by integer multiples of N/K range bins. Comparing the locations of the targets in the combined image with those of the 16 individual channels, similar to the example in Fig. 2, the targets are now divided into three disjoint sets:

(A) matching in every channel
(B) matching in almost ($\gg$50%) every channel
(C) remaining other

In Fig. 10a, targets of group (A) and (B) are marked and will be considered correct targets. Remaining targets are classified as ambiguities and will be ignored. In Fig. 10b, the encircled region of Fig. 10a is magnified for better visualization. It shows that, with one exception, all targets within the range observable by the sensor are emerging in (almost) every channel. In comparison, all but one target of the remaining targets in Fig. 10a are correctly identified as ambiguities.

For each correct target, additionally, the direction of arrival is estimated via an FFT along the virtual channels. This yields the x-y image shown in Fig. 9b. Here, the typical L-shape of the vehicle is clearly discernible. Additionally, reflections of stationary objects are also observable and assignable to the objects in the scene except of a single clutter target.

F. Discussion

The evaluation findings concerning maximum unambiguous range and velocity, Doppler sensitivity, PNR, and PSLL are summarized in Table V. I-OFDM serves as the reference and is therefore rated with neutral (○) in each category. The other approaches are rated relatively to this where the ratings "–",

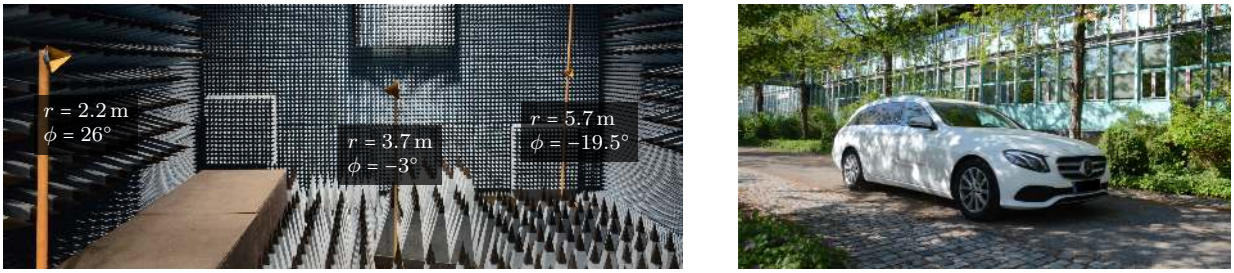

(a) (b)

Fig. 6. Measurement setups. (a) In the anechoic chamber using three static targets and (b) outdoor of an approaching vehicle.

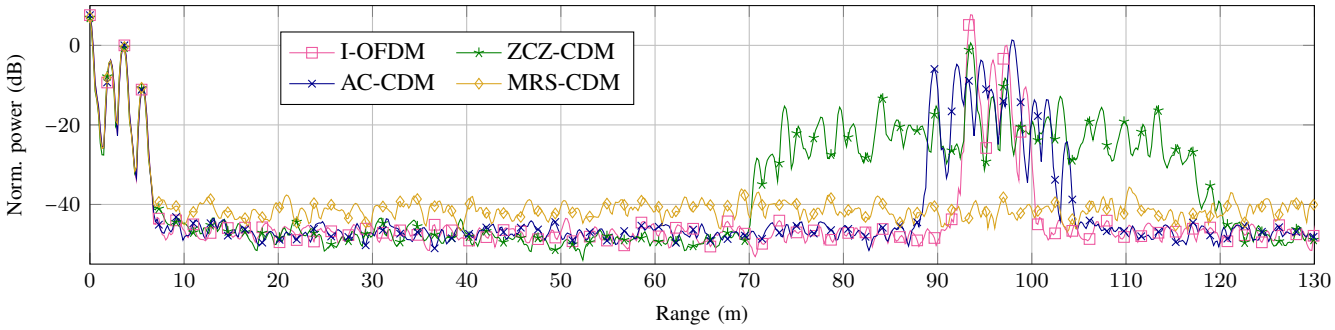

Fig. 7. Range profiles of measurements of the static scene in Fig. 6a using I-OFDM, ZCZ-, AC-, and MRS-CDM.

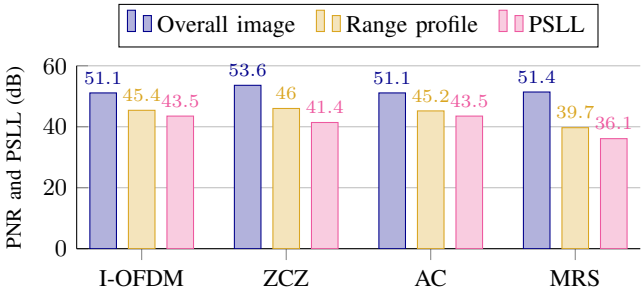

Fig. 8. Achieved PNR of radar images and range profiles and PSLLs of measurements of the static scene.

TABLE V
COMPARISON OVERVIEW OF THE APPROACHES.

	I-OFDM	ZCZ	AC$^+$	MRS
R_{ua}	○	−	+	+
v_{ua}	○	○	○	−
Doppler sensitivity	○	+[1]	○	+[1]
PNR	○	+	○	−
PSLL	○	−	○	−

[1] with ACDC processing

"○", and "+" resemble worse, similar, and better performance than I-OFDM, respectively.

In summary, each approach is able to deliver better results than I-OFDM in at least one property. For ZCZ- and MRS-CDM, this comes at cost of degraded performance of other properties, whereas for AC$^+$-CDM additional steps in target detection are required. Therefore, these approaches should be applied depending on the desired application or scenario. ZCZ-CDM obtains a higher PNR and is less sensitive to Doppler shifts but achieves only $3/4R_{\text{ua}}^{\text{I-OFDM}}$ for the same K. Hence, ZCZ-CDM is an alternative for scenarios with high Doppler but moderate ranges. AC-CDM and I-OFDM, although using quite different signal designs, obtain comparable results regarding performance and limitations. As the number of transmitters increases, resolving ambiguities in AC$^+$ ($N_{\text{guard}}\neq 0$) becomes more challenging and the risk of missing targets increases. Therefore, AC$^+$ is better suited for long range scenarios with a small number of transmitters. With MRS-CDM $R_{\text{ua}}^{\text{max}}$ is obtainable since the range restriction is shifted to the Doppler domain, where this degradation is tolerable up to $K\leq 4$. Hence, MRS is also suited for long range scenarios with a small number of transmitters. In measurements it showed that MRS is sensitive to amplitude scaling, which has to be considered in system design. In general, the CDM approaches allow a higher throughput as all subcarriers are available to all transmitters at all times. This allows more flexibility in signal design and more robustness. Additionally, some of the schemes may be combined in case of large arrays where a single approach would be too restrictive. For instance, consider the combination or MRS and I-OFDM or AC$^+$-CDM for the given signal parameters in Table II and unambiguous ranges in Table IV. Assume a system that should be able to measure targets with velocities up to 55 m/s and with maximum range 150 m. For both MRS, AC$^+$, and I-OFDM, in maximum $K=4$ is reasonable. However, combining I-OFDM with MRS would allow four transmitters to be interleaved and, applying MRS, additionally four transmitters per subcarrier which sums up to 16 transmitters. Similarly, AC may be combined with MRS where AC is applied across the subcarriers and MRS across the OFDM symbols.

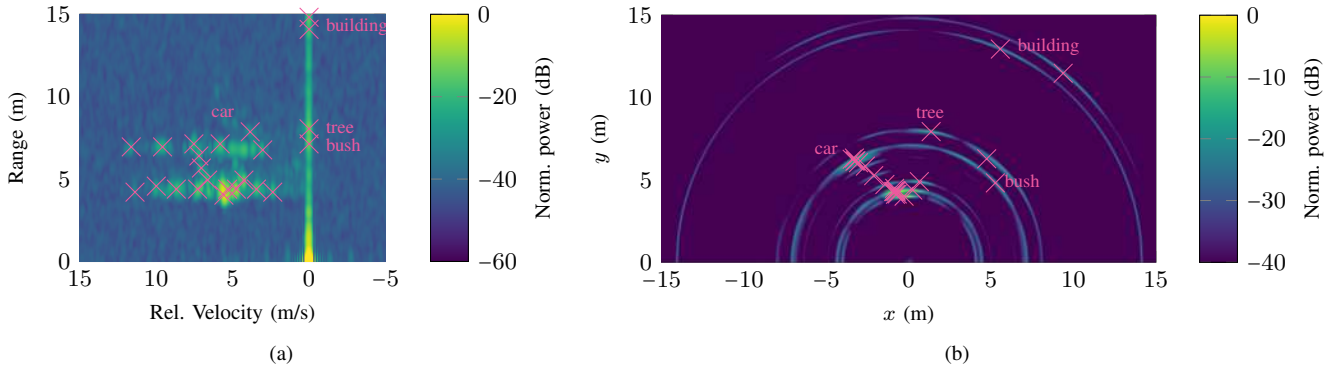

Fig. 9. Measurement of an approaching vehicle using AC-CDM: (a) range-velocity image and (b) range-azimuth image with CFAR detection results (×).

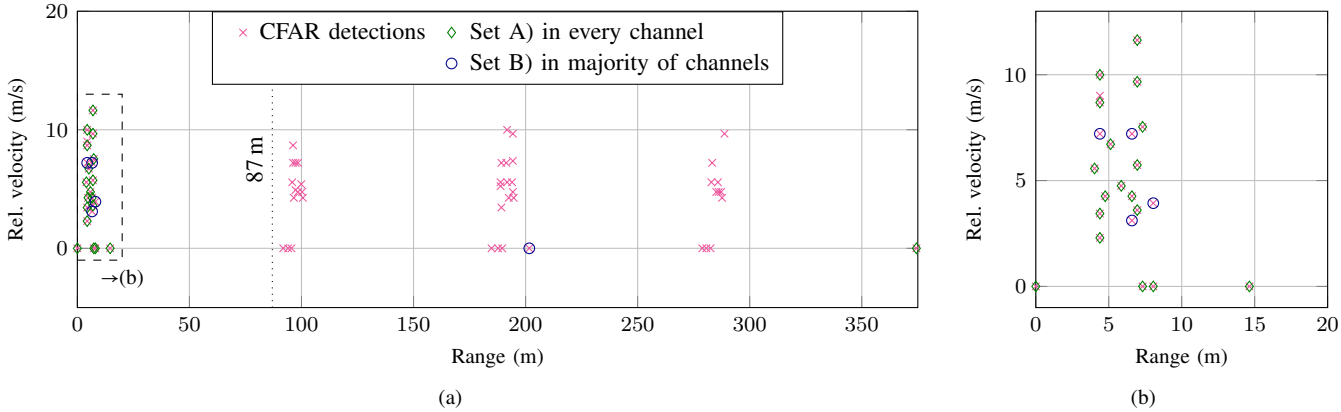

Fig. 10. Detected targets in the overall radar image (a) up to $R_{\mathrm{ua}}^{\mathrm{max}}$ and (b) of the area actually observed by the sensor (=area where targets are expected).

VI. Conclusion

In this paper, the opportunity of utilizing the coding within OFDM symbols for MIMO is suggested and examined. It shows that the simple naive coding approach suffers from low PNR due to the high cross-correlation of the waveforms. Therefore, three novel strategies are proposed that aim at reducing or eliminating the cross-correlation of interfering transmitters. As perfect orthogonal coded waveforms do not exist, a trade-off has to be made between good isolation between the channels and ambiguities in the radar evaluation. Despite these constraints, it is shown that the approaches constitute competitive alternatives to the common I-OFDM. Moreover, the suggested approaches offer different alternatives where the inevitable constraints occur. For instance, in AC-CDM, ambiguities in range emerge where their locations may be controlled in the signal design, whereas for MRS ambiguities emerge in Doppler instead of in range. This introduces a much wider variety of possible waveforms with different and more diverse characteristics. It is therefore also suggested that the approaches may be combined, especially for larger arrays as in this case, the constraints can be divided into several dimensions, thus avoiding severe limitations in a single dimension.

References

[1] F. Roos, J. Bechter, C. Knill, B. Schweizer, and C. Waldschmidt, "Radar Sensors for Autonomous Driving: Modulation Schemes and Interference Mitigation," *IEEE Microw. Mag.*, vol. 20, no. 9, pp. 58–72, Sep. 2019.

[2] J. Li and P. Stoica, "MIMO Radar with Colocated Antennas," *IEEE Signal Process. Mag.*, vol. 24, no. 5, pp. 106–114, Sep. 2007.

[3] H. Sun, F. Brigui, and M. Lesturgie, "Analysis and comparison of MIMO radar waveforms," in *Int. Radar Conf.* IEEE, Oct. 2014, pp. 1–6.

[4] N. Levanon and E. Mozeson, "Multicarrier Radar Signal–Pulse Train and CW." *IEEE Trans. Aerosp. Electron. Syst*, vol. 38, no. 2, pp. 707–720, Apr. 2002.

[5] C. Sturm and W. Wiesbeck, "Waveform Design and Signal Processing Aspects for Fusion of Wireless Communications and Radar Sensing," *Proc. IEEE*, vol. 99, no. 7, pp. 1236–1259, 2011.

[6] D. Schindler, B. Schweizer, C. Knill, J. Hasch, and C. Waldschmidt, "An Integrated Stepped-Carrier OFDM MIMO Radar Utilizing a Novel Fast Frequency Step Generator for Automotive Applications," *IEEE Trans. Microw. Theory Techn.*, vol. 67, no. 11, pp. 4559–4569, Nov. 2019.

[7] A. Bourdoux, U. Ahmad, D. Guermandi, S. Brebels, A. Dewilde, and W. Van Thillo, "PMCW waveform and MIMO technique for a 79 GHz CMOS automotive radar," *Proc. IEEE Radar Conf.*, 2016.

[8] C. Sturm, Y. L. Sit, M. Braun, and T. Zwick, "Spectrally interleaved multi-carrier signals for radar network applications and multi-input multi-output radar," *IET Radar, Sonar & Navigation*, vol. 7, no. 3, pp. 261–269, Mar. 2013.

[9] C. Knill, F. Roos, B. Schweizer, D. Schindler, and C. Waldschmidt, "Random Multiplexing for an MIMO-OFDM Radar With Compressed Sensing-Based Reconstruction," *IEEE Microw. Wireless Compon. Lett*, vol. 29, no. 4, pp. 300–302, Apr. 2019.

[10] G. Hakobyan, M. Ulrich, and B. Yang, "OFDM-MIMO Radar With Optimized Nonequidistant Subcarrier Interleaving," *IEEE Trans. Aerosp. Electron. Syst.*, vol. 56, no. 1, pp. 572–584, Feb. 2020.

[11] X. Song, S. Zhou, and P. Willett, "Reducing the Waveform Cross Correlation of MIMO Radar With Space-Time Coding," *IEEE Trans. Signal Process.*, vol. 58, no. 8, pp. 4213–4224, Aug. 2010.

[12] L. Welch, "Lower bounds on the maximum cross correlation of signals (Corresp.)," *IEEE Trans. Inf. Theory*, vol. 20, no. 3, pp. 397–399, May 1974.

[13] J. Overdevest, F. Jansen, F. Uysal, and A. Yarovoy, "Doppler Influence on Waveform Orthogonality in 79 GHz MIMO Phase-Coded Automotive Radar," *IEEE Trans. Veh. Technol*, vol. 69, no. 1, pp. 16–25, Jan. 2020.
[14] T. Hayashi, Y. Watanabe, Anh Pham, T. Miyazaki, S. Matsufuji, and T. Maeda, "A Novel Class of QPSK Zero-Correlation Zone Sequence Sets," in *Seventh International Workshop on Signal Design and its Applications in Communications (IWSDA)*, Sep. 2015, pp. 205–208.
[15] X. Tang and W. H. Mow, "A New Systematic Construction of Zero Correlation Zone Sequences Based on Interleaved Perfect Sequences," *IEEE Trans. Inf. Theory*, vol. 54, no. 12, pp. 5729–5734, Dec. 2008.
[16] H. Haderer, R. Feger, C. Pfeffer, and A. Stelzer, "Millimeter-Wave Phase-Coded CW MIMO Radar Using Zero- and Low-Correlation-Zone Sequence Sets," *IEEE Trans. Microw. Theory Techn.*, vol. 64, no. 12, pp. 4312–4323, Dec. 2016.
[17] G. Hakobyan, M. Girma, X. Li, N. Tammireddy, and B. Yang, "Repeated Symbols OFDM-MIMO Radar at 24 GHz," in *Proc. 13th Eur. Radar Conf.*, 2016.
[18] W. van Rossum and L. Anitori, "Doppler ambiguity resolution using random slow-time code division multiple access MIMO radar with sparse signal processing," in *IEEE Radar Conf.* IEEE, Apr. 2018, pp. 0441–0446.
[19] B. Farley, J. McGrath, and C. Erdmann, "An All-Programmable 16-nm RFSoC for Digital-RF Communications," *IEEE Micro*, vol. 38, no. 2, pp. 61–71, Mar. 2018.
[20] G. Franken, H. Nikookar, and P. van Genderen, "Doppler Tolerance of OFDM-Coded Radar Signals," in *Proc. 3rd Eur. Radar Conf.*, vol. 9, 2006, pp. 108–111.
[21] G. Hakobyan and B. Yang, "A Novel Intercarrier-Interference Free Signal Processing Scheme for OFDM Radar," *IEEE Trans. Veh. Technol*, vol. 67, no. 6, pp. 5158–5167, Jun. 2018.